Smart Materials and Structures

PAPER

Research on backstepping adaptive sliding mode control of digital piezoelectric two-stage proportional valve

To cite this article: Linfei Li *et al* 2025 *Smart Mater. Struct.* **34** 105022

IOP Publishing Smart Materials and Structures
Smart Mater. Struct. **34** (2025) 105022 (14pp) https://doi.org/10.1088/1361-665X/ae0bd0

Research on backstepping adaptive sliding mode control of digital piezoelectric two-stage proportional valve

Linfei Li[1], Yuwen Wang[1,2], Yuchuan Zhu[1,*] and Jie Ling[1]

[1] College of Mechanical and Electrical Engineering, Nanjing University of Aeronautics and Astronautics, Nanjing 210016, People's Republic of China
[2] Nanjing Chenguang Group Industrial Co.,Ltd., Nanjing 210006, People's Republic of China

E-mail: meeyczhu@nuaa.edu.cn

Received 8 July 2025, revised 8 September 2025
Accepted for publication 24 September 2025
Published 16 October 2025

Abstract

Adapting to the growing trend of digitalization, intelligence, and electrification in engineering vehicles, a high-frequency response and highly reliable digital piezoelectric two-stage proportional valve (DPPV) is proposed and verified. The structure and working principle of the DPPV are described, and its nonlinear dynamic mathematical model is established. Aiming at the influence of serious nonlinearity, time-varying and unmodeled factors on the displacement control performance of DPPV, a backstepping adaptive sliding mode control strategy is proposed. The simulation model of the DPPV and its controller is constructed by Simulink, and the spool displacement tracking effect of the valve under step and sinusoidal input signals is analyzed. A DPPV test bench is built, and the tracking performance under three sinusoidal conditions (covering different displacement amplitudes and frequencies) is investigated experimentally. The experimental results show that, compared with the traditional PWM control strategy, the control method reduces at least 12.3%, 40.8% and 37.7% in terms of the maximum, average and standard deviation of the tracking error, respectively. In addition, the control effect of the digital electromagnetic two-stage proportional valve is compared and analyzed. The results show that the maximum error, average error and mean square error of the proposed structure power main spool displacement tracking (tracking curve: $x = 4.5\sin(3\pi t)$) are improved by 64.1%, 40.35% and 70%, respectively, which further verifies its superiority under complex working conditions. This research not only provides a new theoretical basis and design ideas for the development of large flow digital proportional valves, but also expands a new direction for the application of digital hydraulic components in a wider range of fields.

Keywords: digital piezoelectric two-stage proportional valve, backstepping adaptive sliding mode control strategy, digital electromagnetic two-stage proportional valve, nonlinearity

* Author to whom any correspondence should be addressed.

1. Introduction

As the core power transmission system of construction vehicles, the hydraulic transmission system with significant technical advantages such as a compact structure, high power density and flexible dynamic response has long provided important support for the efficient operation of construction machinery [1, 2]. Yet, as the key control element of the system, the hydraulic control valve has the technical limitations of insufficient control accuracy and low digital integration, which has become the main bottleneck restricting the automation and intelligent upgrading of traditional construction engineering vehicles (such as concrete pump trucks, cranes, etc) [3–7]. The digital two-stage valve driven by a high-speed on/off valve, which integrates discrete digital hydraulic technology, electrical sensing technology and integrated design technology, has the advantages of high frequency response, zero leakage, digital drive and intelligent control [8, 9]. It has become a research hotspot in the digitalization and intelligence of hydraulic components for construction machinery at present [10, 11].

At the beginning of the 21st century, foreign countries began to study the PDV with high-speed on/off valve as the pilot stage, and rapidly promoted its commercialization process. In 2004, Parker Company took the lead in introducing the VPL series multi-way valve [12]. The valve uses two two-position three-way high-speed on/off valves as the pilot stage to drive the main spool to achieve loop control. In 2008, Eaton Corporation of the United States, with the comprehensive application of load port independent control technology, high-speed on/off valve technology and mechatronics technology, innovatively adopted two two-position three-way voice coil motor direct drive pilot valves to drive two power main spools respectively [13–15]. In 2011, Danish company Danfoss developed the PVG series of load-sensitive proportional multi-valves [16]. The pilot stage of this valve employs four high-speed on/off valves arranged in a bridge circuit to regulate the operating state of the main power spool. By 2017, Danfoss had once again innovated with the development of the PVX series multi-way valves, sharing structural design similarities with the Eaton ZTS series valves from the United States. Nonetheless, the PVX series takes it a step further by incorporating an additional temperature sensor, besides to the already integrated displacement and pressure sensors [17, 18].

In China, the application of high-speed on/off valves as pilot stages in the research field of electro-hydraulic two-stage valves started relatively late. In 2017, Zhong Qi from Zhejiang University innovatively proposed a new digital proportional valve, consisting of four two-position three-way high-speed on/off valves and two three-position three-way main spools, based on the structural configuration of Eaton ZTS16 series multi-way valves [19, 20]. Simulation and experimental results demonstrate that the digital proportional valve exhibits superior dynamic performance compared to traditional proportional valves and servo valves. In 2020, Xu Long of Lanzhou University of Science and Technology proposed a pilot-operated high-flow, high-speed on/off valve unit and utilized four of these units to cleverly construct a three-position, four-way functioning water-pressure proportional valve by means of a bridging circuit, which further pushed forward the technological development in this field [21, 22]. In 2021, Gao Qiang from Nanjing University of Aeronautics and Astronautics introduced a two-stage electro-hydraulic proportional valve, which utilizes an array of high-speed on/off valves in a 'B + B' type hydraulic full-bridge pilot regulation system. They further implemented a sliding mode controller for the position control of the main spool, enabling high-precision manipulation of the power main spool [23]. In 2022, Ruihao Zhao from Taiyuan University of Technology developed a high-performance water based proportional directional valve with high-speed on/off valve pilot control. This design leverages high-speed on/off valve technology and the displacement flow feedback principle [24–26].

The above research results further reveal that the digital proportional two-stage valve with a high-speed on/off valve featuring fluid discrete characteristics as the pilot stage shows great application potential to replace the traditional proportional/servo control system valves. At present, most PDVs adopt electromagnetic high-speed on/off valves as the pilot drive components. However, due to the inherent working principle of electromagnetic high-speed on/off valves, there are inevitably significant electromagnetic hysteresis and mechanical hysteresis [27]. This hysteresis characteristic limits dynamic performance. It negatively impacts the speed and resolution of fluid discrete. This becomes a key bottleneck for improving control accuracy and the dynamic response speed of the PDV valve core displacement [28]. Piezoelectric stacks exhibit two main benefits: high frequency response characteristics and generate strong output force [29–31]. It is used in the electromechanical converter of the high-speed on/off valve to form a piezoelectric high-speed on/off valve. It can effectively fix the issues of the electromagnetic high-speed on/off valve, like mechanical response and electromagnetic lag [32].

This manuscript presents a plan to replace the nozzle–flapper variable throttle port with a piezoelectric high-speed on/off valve. This new design is based on the nozzle–flapper servo valve. The goal is to improve control accuracy, reliability, and the long service life of traditional hydraulic valves. It also aims to maintain their high-frequency dynamic response. In view of the severe nonlinearity, time-varying and unmodeled parameters of the digital piezoelectric two-stage valve that adversely affect the control characteristics of the spool displacement, a backstepping adaptive sliding mode control strategy is further proposed. Through simulation and experiments, the feasibility of the proposed digital piezoelectric two-stage valve scheme and the effectiveness of the control strategy are explored under step and sinusoidal signal tracking conditions.

The residual structural of this paper is organized as follows. The description of the proposed valve is presented in section 2. The nonlinear modeling and characteristics analysis is demonstrated in section 3. A backstepping adaptive control strategy is designed in section 4. Simulation modeling and analysis are discussed in section 5. The experimental investigations are

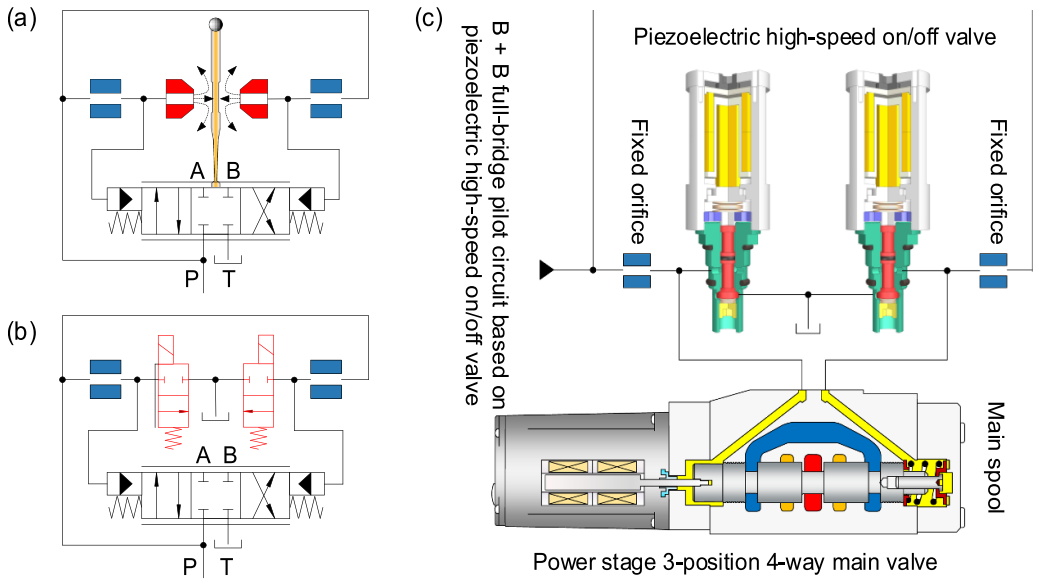

Figure 1. Digital piezoelectric two-stage proportional valve structure diagram.

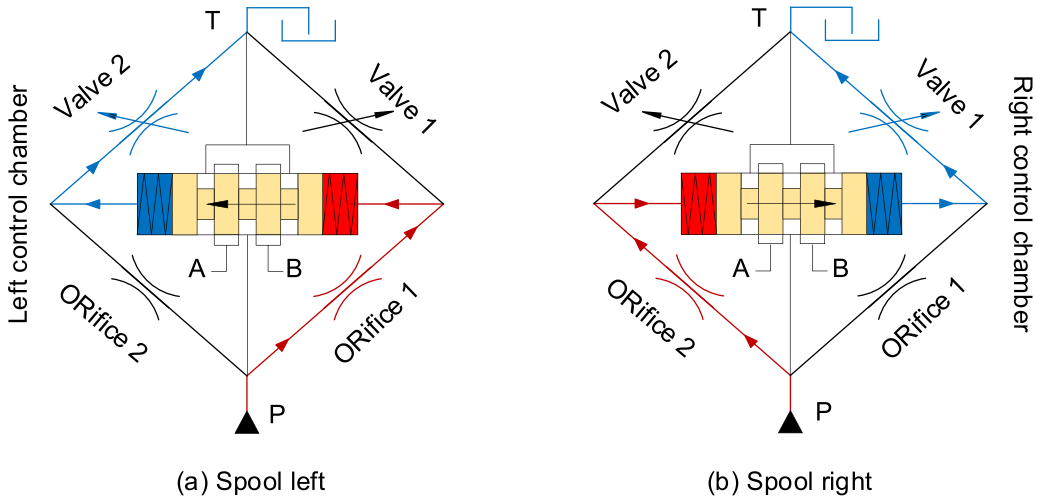

Figure 2. The working principle diagram of digital piezoelectric proportional two-stage valve.

presented in section 6. The overall discussion and conclusions is given in section 7.

2. Structure and principle of operation

Figure 1 shows the structure diagram of the digital piezoelectric proportional two-stage valve (DPPV). This valve is driven by a piezoelectric high-speed on/off valve, as proposed in this study. It can be seen from the diagram that on the basis of the structure of the flapper–nozzle servo valve. The piezoelectric high-speed on/off valve with the advantages of strong anti-pollution ability, high dynamic response, and zero leakage, is replaced by the nozzle flapper, thus constituting a DPPV, whose structural sketch is shown in figure 1(b). Compared with the traditional flapper–nozzle servo valve (as shown in figure 1(a)), this application completely replaces the nozzle flapper pre-stage with high failure rate in the flapper–nozzle servo valve. It not only realizes the digital drive, high reliability and long service life of the digital piezoelectric two-stage servo valve, but also retains its original dynamic characteristics, and the specific structure as shown in figure 1(c). Note that to verify the feasibility of the DPPV, the three-position four-way power main valve from Jiangsu Hengli Co., Ltd is chosen, considering cost and processing difficulty.

The working principle of the DPPV is illustrated in figure 2. When the piezoelectric high-speed on/off valve 1 is activated and valve 2 is not, the pressure in the control chamber on the left side of the main spool decreases, while the right side maintains high pressure. This pressure difference causes the main spool to move to the left. Conversely, when the main spool moves to the right, the piezoelectric high speed on/off valve 1 is deactivated, and valve 2 is activated.

3. Mathematical modeling

3.1. Pilot-level mathematical modeling

The DPPV mainly consists of two fixed orifices and two piezoelectric high-speed on/off valves. The flow equations for the two fixed orifices are as follows:

$$q_{j1} = C_j A_j \sqrt{\frac{2(p_s - p_a)}{\rho}} = C_j \frac{\pi d_j^2}{4} \sqrt{\frac{2(p_s - p_a)}{\rho}} \tag{1}$$

$$q_{j2} = C_j A_j \sqrt{\frac{2(p_s - p_b)}{\rho}} = C_j \frac{\pi d_j^2}{4} \sqrt{\frac{2(p_s - p_b)}{\rho}} \tag{2}$$

where d_j is the diameter of the fixed orifice, A_j is the flow area of the fixed orifice, C_j is the flow coefficient, p_s is the pilot supply pressure, p_a is the pressure of the left control chamber of the main valve stage, and p_b is the pressure of the right control chamber of the main valve stage. The flow equations for the piezoelectric high-speed on/off valves HSV1 and HSV2 are as follows:

$$q_{h1} = C_d A_p (\tau_0 - \tau) \sqrt{\frac{2p_a}{\rho}} \tag{3}$$

$$q_{h2} = C_d A_p (\tau_0 + \tau) \sqrt{\frac{2p_b}{\rho}} \tag{4}$$

where C_d is the flow coefficient of the piezoelectric high-speed on/off valve, A_p is the flow area of the piezoelectric high-speed on/off valve, and τ is the PWM duty cycle.

Ignoring the leakage of the main valve, and taking the case where the main valve ($x_v > 0$) moves to the right as an example, the flow continuity equations of the left and right control chambers of the main valve are as follows:

$$\dot{p}_a = \frac{\beta_e}{V_0 + A_v x_v} \left((q_{j1} - q_{h1}) - A_v \dot{x}_v \right) \tag{5}$$

$$\dot{p}_b = \frac{\beta_e}{V_0 - A_v x_v} \left(A_v \dot{x}_v - (q_{h2} - q_{j2}) \right) \tag{6}$$

where V_0 is the initial volume of the control chamber on each side, A_v is the cross-sectional area of the main valve, β_e is the elastic modulus of the oil, and x_v is the displacement of the main valve.

3.2. Mathematical modeling of the main spool

The dynamic equation of the main valve spool is:

$$m_v \ddot{x}_v = (p_a - p_b) A_v - k_v x_v - B_v \dot{x}_v - F_{vf} - F_{vs} \tag{7}$$

where m_v is the equivalent mass of the main valve, B_v is the viscous damping coefficient of the main valve, k_v is the stiffness of the centering spring, F_{vf} is the friction force, and F_{vs} is the steady-state hydrodynamic force acting on the main valve.

The main valve port has a U-shaped configuration. Assuming there are n valve ports on each control side, the flow area of the valve port is [33]:

$$A_k = \begin{cases} nR_v^2 \left[\arccos\left(1 - \frac{x_v - \Delta}{R_v}\right) - \left(1 - \frac{x_v - \Delta}{R_v}\right) \sqrt{\frac{x_v - \Delta}{R_v}\left(2 - \frac{x_v - \Delta}{R_v}\right)} \right] & 0 \leqslant x_{v0} \leqslant R_v \\ \frac{\pi n R_v^2}{2} + 2nR_v (x_v - \Delta - R_v) & R_v < x_{v0} \end{cases} \tag{8}$$

where R_v is the radius of the U-shaped valve port, Δ is the median dead zone of the main valve spool, x_{v0} is the length of the U-shaped valve port. The flow through the main valve port can be expressed as:

$$q_v = n C_{vd} A_k \sqrt{\frac{2\Delta p_v}{\rho}} \tag{9}$$

where C_{vd} is the flow coefficient of the U-shaped valve port, Δp_v the pressure difference of the main valve port.

$$F_{ms} = 2n C_{vv} C_{vd} A_k \Delta p_v \cos\theta_v \tag{10}$$

where C_{vv} is the velocity coefficient of the U-shaped valve port, and θ_v is the jet angle of the main valve port.

4. Control strategy

The main valve position servo control system of the two-stage electro-hydraulic proportional valve, featuring high-speed on/off valve pilot control, faces challenges such as nonlinear characteristics and parameter uncertainty. When the system undergoes long-term operation, leading to fluctuations in performance parameters or exposure to large external disturbances, the effectiveness of the traditional PID control strategy tends to diminish [34–36]. To address this, an innovative backstepping adaptive sliding mode control strategy is proposed in this paper. This strategy effectively combines the strengths of backstepping and adaptive sliding mode control technology, aiming to mitigate the adverse effects of system nonlinearity and parameter uncertainty, thereby enhancing the robustness of system control, as show figure 3.

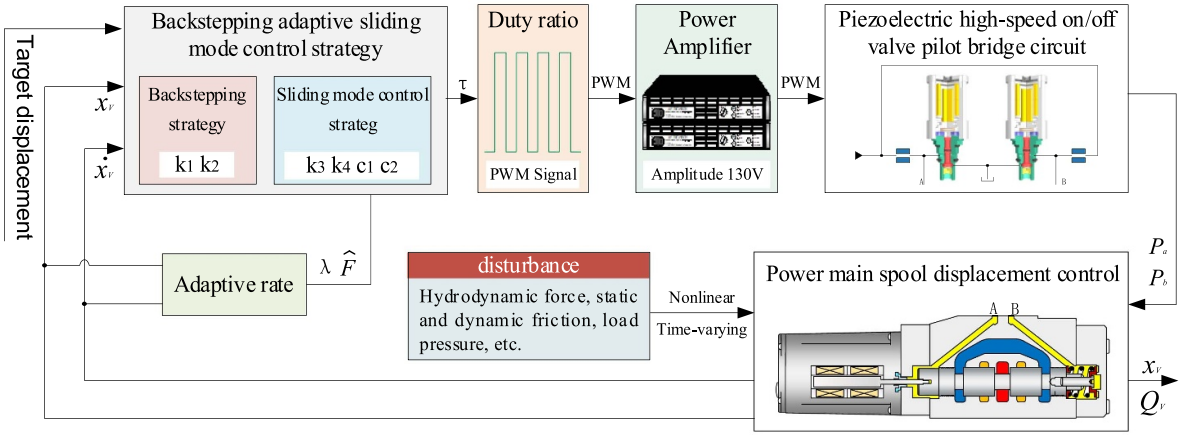

Figure 3. Block diagram DPPV inverse step size adaptive sliding mode control.

The linearization equation of the pilot bridge for the piezoelectric high-speed on/off valve at a 0.5 duty cycle is as follows:

$$q_{\mathrm{L}} = K_{\mathrm{q0}}\tau - K_{\mathrm{c0}}p_{\mathrm{L}} \tag{11}$$

where K_{q0} is the flow gain, K_{c0} is the flow-pressure coefficient, $K_{\mathrm{q0}} = C_{\mathrm{d}}A\sqrt{\frac{p_{\mathrm{s}}}{\rho}}$, $K_{\mathrm{c0}} = \frac{\tau_0 C_{\mathrm{d}}A}{\sqrt{p_{\mathrm{s}}\rho}}$.

According to equations (5) and (6), the flow continuity equation for the main valve control chamber can be expressed as follow:

$$q_{\mathrm{L}} = \frac{(Q_{\mathrm{j1}} - Q_{\mathrm{h1}}) + (Q_{\mathrm{h2}} - Q_{\mathrm{j2}})}{2} = A_{\mathrm{v}}\dot{x}_{\mathrm{v}} + \frac{V_0}{2\beta_{\mathrm{e}}}\left(\dot{p}_{\mathrm{a}} - \dot{p}_{\mathrm{b}}\right) + \frac{A_{\mathrm{v}}x_{\mathrm{v}}}{2\beta_{\mathrm{e}}}\left(\dot{p}_{\mathrm{a}} + \dot{p}_{\mathrm{b}}\right). \tag{12}$$

Since $A_{\mathrm{v}}x_{\mathrm{v}} \ll V_0$ and $\dot{p}_{\mathrm{a}} + \dot{p}_{\mathrm{b}}$ then equation (12) can be simplified as:

$$q_{\mathrm{L}} = A_{\mathrm{v}}\dot{x}_{\mathrm{v}} + \frac{V_0}{2\beta_{\mathrm{e}}}\dot{p}_{\mathrm{L}}. \tag{13}$$

Considering unmodeled factors and the presence of interference, the dynamic for the main valve is as follows:

$$m_{\mathrm{v}}\ddot{x}_{\mathrm{v}} = p_{\mathrm{L}}A_{\mathrm{v}} - B_{\mathrm{v}}\dot{x}_{\mathrm{v}} - k_{\mathrm{v}}x_{\mathrm{v}} - f \tag{14}$$

where f is an unknown disturbance force, which mainly includes steady-state hydrodynamic force, friction force, modeling error and other disturbances.

The derivation of equation (14) is obtained:

$$\dddot{x}_{\mathrm{v}} = \frac{A_{\mathrm{v}}}{m_{\mathrm{v}}}\dot{p}_{\mathrm{L}} - \frac{B_{\mathrm{v}}}{m_{\mathrm{v}}}\ddot{x}_{\mathrm{v}} - \frac{k_{\mathrm{v}}}{m_{\mathrm{v}}}\dot{x}_{\mathrm{v}} - \frac{\dot{f}}{m_{\mathrm{v}}}. \tag{15}$$

Substituting equations (12) and (13) into equation (15):

$$\begin{aligned}\dddot{x}_{\mathrm{v}} &= \frac{2A_{\mathrm{v}}\beta_{\mathrm{e}}}{m_{\mathrm{v}}V_0}\left(K_{\mathrm{v}}\tau - K_{\mathrm{c}}p_{\mathrm{L}} - A_{\mathrm{v}}\dot{x}_{\mathrm{v}}\right) - \frac{B_{\mathrm{v}}}{m_{\mathrm{v}}}\ddot{x}_{\mathrm{v}} - \frac{k_{\mathrm{v}}}{m_{\mathrm{v}}}\dot{x}_{\mathrm{v}} - \frac{\dot{f}}{m_{\mathrm{v}}} \\ &= -\frac{B_{\mathrm{v}}}{m_{\mathrm{v}}}\ddot{x}_{\mathrm{v}} - \left(\frac{k_{\mathrm{v}}}{m_{\mathrm{v}}} + \frac{2A_{\mathrm{v}}{}^2\beta_{\mathrm{e}}}{m_{\mathrm{v}}V_0}\right)\dot{x}_{\mathrm{m}} + \frac{2A_{\mathrm{v}}\beta_{\mathrm{e}}}{m_{\mathrm{v}}V_0}K_{\mathrm{v}}\tau \\ &\quad - \frac{\dot{f}}{m_{\mathrm{v}}} - \frac{2A_{\mathrm{v}}\beta_{\mathrm{e}}}{m_{\mathrm{v}}V_0}K_{\mathrm{c}}p_{\mathrm{L}}.\end{aligned} \tag{16}$$

Taking the state quantity $x_1 = x_2$, $x_2 = \dot{x}_{\mathrm{v}}$ and $x_3 = \ddot{x}_{\mathrm{v}}$, x_1, x_2 and x_3 as the displacement, velocity and acceleration of the main valve respectively, the state space expression of the system is obtained according to the formula (16) as follows:

$$\begin{cases} \dot{x}_1 = x_2 \\ \dot{x}_2 = x_3 \\ \dot{x}_3 = a_3x_3 + a_2x_2 + a_1\tau + F \end{cases} \tag{17}$$

where $a_1 = \frac{2A_{\mathrm{v}}\beta_{\mathrm{e}}}{m_{\mathrm{v}}V_0}K_{\mathrm{v}}$, $a_2 = -\frac{K_{\mathrm{v}}}{m_{\mathrm{v}}} - \frac{2A_{\mathrm{v}}^2\beta_{\mathrm{e}}}{m_{\mathrm{v}}V_0}$, $a_3 = -\frac{B_{\mathrm{v}}}{m_{\mathrm{v}}}$, $F = -\frac{\dot{f}}{m_{\mathrm{v}}} - \frac{2A_{\mathrm{v}}\beta_{\mathrm{e}}}{m_{\mathrm{v}}V_0}K_{\mathrm{c}}p_{\mathrm{L}}$.

The position error of the main valve is defined as:

$$e_1 = x_1 - x_{1\mathrm{d}} \tag{18}$$

where $x_{1\mathrm{d}}$ is ideal position for main valve. Derivation of equation (18),

$$\dot{e}_1 = x_1 - \dot{x}_{1\mathrm{d}} = x_2 - \dot{x}_{1\mathrm{d}}. \tag{19}$$

The Lyapunov function is taken as:

$$V_1 = \frac{1}{2}e_1{}^2 \geqslant 0. \tag{20}$$

Derivation of equation (20):

$$\dot{V}_1 = e_1\,\dot{e}_1 = e_1\left(x_2 - \dot{x}_{1\mathrm{d}}\right). \tag{21}$$

Define the error variable $e_2 = x_2 - x_{2d}$, where x_{2d} is the virtual control variable,

$$x_{2d} = x_{1d} - k_1 e_1. \tag{22}$$

Substitute (22) into (21) to get:

$$\dot{V}_1 = -k_1 {e_1}^2 + e_1 e_2. \tag{23}$$

Derivation of e_2:

$$\dot{e}_2 = \dot{x}_2 - \dot{x}_{2d} = x_3 - \dot{x}_{2d}. \tag{24}$$

The Lyapunov function is taken as:

$$V_2 = V_1 + \frac{1}{2}{e_2}^2 \geqslant 0. \tag{25}$$

Derivation of equation (25):

$$\dot{V}_2 = \dot{V}_1 + e_2 e_2 = -k_1 e_1 + e_1 e_2 + e_2 (x_3 - \dot{x}_{2d}). \tag{26}$$

Define the error variable $e_3 = x_3 - x_{3d}$, where x_{3d} is the virtual control variable, and take:

$$x_{3d} = -e_1 + \dot{x}_{2d} - k_2 e_2. \tag{27}$$

Substitute (27) into (26) to get:

$$\dot{V}_2 = -k_1 {e_1}^2 - k_2 {e_2}^2 + e_2 e_3 \tag{28}$$

where k_1 and k_2 are the parameters of the backstepping method. Combining backstepping method with sliding mode control, the sliding mode surface is defined as:

$$s = c_1 e_1 + c_2 e_2 + e_3 \tag{29}$$

which c_1 and c_2 are sliding surface parameters. Derivation of equation (29):

$$\dot{s} = c_1 \dot{e}_1 + c_2 \dot{e}_2 + \dot{x}_3 - \dot{x}_{3d}. \tag{30}$$

Substitute (17) into (30) to get:

$$\dot{s} = c_1 \dot{e}_1 + c_2 \dot{e}_2 + a_3 x_3 + a_2 x_2 + a_1 \tau + F - \dot{x}_{3d}. \tag{31}$$

The Lyapunov function is taken as:

$$V_3 = V_2 + \frac{1}{2}s^2 \geqslant 0. \tag{32}$$

Derivation of equation (32):

$$\dot{V}_3 = -k_1 {e_1}^2 - k_2 {e_2}^2 + e_2 e_3 + s[c_1 \dot{e}_1 + c_2 \dot{e}_2 + a_3 x_3 + a_2 x_2 + a_1 \tau + F - \dot{x}_{3d}]. \tag{33}$$

From equation (33), it can be seen that F is related to both the hydrodynamic force, friction and load pressure on the main valve. It is difficult to calculate F directly and accurately without using pressure sensors to measure the pressure in the two chambers of the main valve. Therefore, this paper considers that F has parametric uncertainty and defines $\tilde{F} = F - \hat{F}$, where $\tilde{F}$ is the estimated value of F and $\tilde{F}$ is the estimation error.

The Lyapunov function is taken as:

$$V_4 = V_3 + \frac{1}{2}\lambda \tilde{F}^2 \geqslant 0. \tag{34}$$

Derivation of equation (34):

$$V_4 = -k_1 {e_1}^2 - k_2 {e_2}^2 + e_2 e_3 + s[c_1 \dot{e}_1 + c_2 \dot{e}_2 + a_3 x_3 + a_2 x_2 + a_1 \tau + F - \dot{x}_{3d}] - \lambda. \tag{35}$$

The sliding mode controller is taken as:

$$\tau = \frac{1}{a_1}\left[-c_1 \dot{e}_1 - c_2 \dot{e}_2 - a_3 x_3 - a_2 x_2 - \hat{F} + \dot{x}_{3d} - k_3 s - k_4 \operatorname{sgn}(s)\right]. \tag{36}$$

The adaptive law of parameters is:

$$\dot{\hat{F}} = \frac{s}{\lambda} \tag{37}$$

where λ is the adaptive law parameter. Substitute (37) into (36) to get:

$$V_4 = -k_1 {e_1}^2 - k_2 {e_2}^2 + e_2 e_3 - k_3 s^2 - k_4 |s| = -E^{\mathrm{T}} Q E - k_4 |s| \tag{38}$$

$$E = [e_1, e_2, e_3]^{\mathrm{T}} \tag{39}$$

$$Q = \begin{bmatrix} k^1 + k^1 e_1^2 & c_1 k_1 k_2 & c_1 k_3 \\ c_1 c_2 k_3 & k_2 + k_3 c_2^2 & c_2 k_3 - \frac{1}{2} \\ c_1 k_3 & c_2 k_3 - \frac{1}{2} & k_3 \end{bmatrix}. \tag{40}$$

When the first-order, second-order and third-order principal sub-formulas of matrix $\boldsymbol{Q}$ are all greater than 0, that is, when the conditions of equation (37) are satisfied, matrix $\boldsymbol{Q}$ is a positive definite matrix. According to the Lyapunov stability criterion, it can be judged that the adaptive backstepping sliding mode controller of the two-stage electro-hydraulic proportional valve is asymptotically stable. Therefore, the main valve can gradually track the target displacement [37], which indicates that the adaptive backstepping sliding mode controller can theoretically realize the position servo control of the main valve,

$$\begin{cases} d_i > 0 (i = 1,2,3)\ , c_1 > 0\ , c_2 > 0 \\ k_1 k_2 + k_1 k_3 {c_2}^2 + k_2 k_3 {c_1}^2 > 0 \\ k_1 k_2 k_3 + k_1 k_3 c_2 - (k_1 + k_3 c_1)/4 > 0 \end{cases}. \tag{41}$$

5. Simulation modeling and analysis

The simulation model of adaptive backstepping sliding mode controller is built in by MATLAB/Simulink, as shown in figure 4. Based on the Lsight software platform and the MATLAB model of the DPPV, a genetic algorithm is employed to minimize the valve spool displacement error

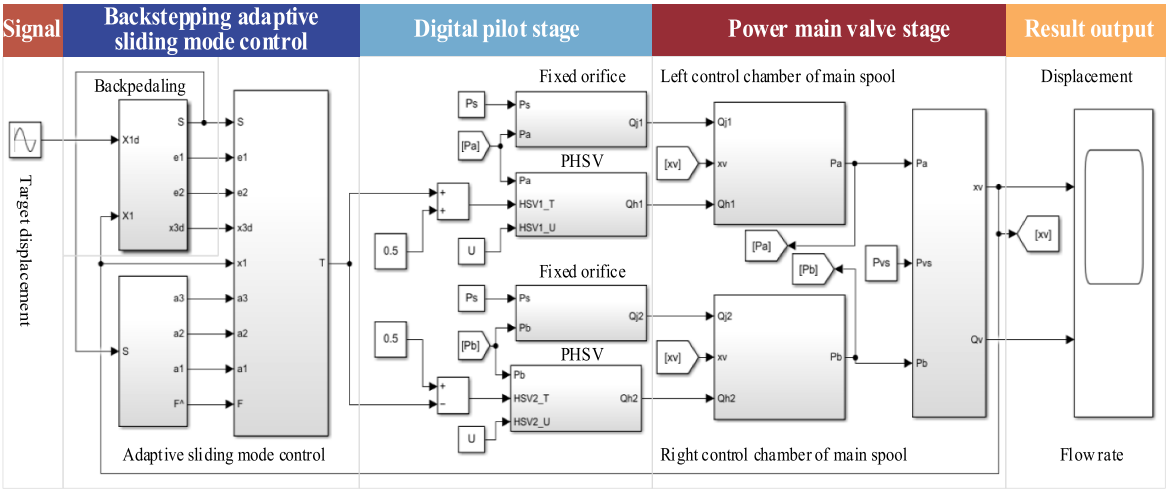

Figure 4. Block diagram DPPV inverse step size adaptive sliding mode control.

Table 1. The setting of some key parameters in the simulation model.

Name	Sign	Valve
The flow coefficient of fixed orifice (mm)	C_j	0.7
The diameter of fixed orifice (mm)	d_j	0.8
The initial volume of control cavity (mm^3)	V_0	3750
The effective working cross-sectional area of the main valve (mm^2)	A_v	200
The mass of main valve (kg)	m_v	0.2
The viscous damping coefficient of main valve ($N\ (m \cdot s)^{-1}$)	B_v	17.6
The stiffness of the centering spring ($N\ mm^{-1}$)	k_v	50
The frictional force of the main valve (N)	F_{vf}	8
The number of radial distribution valve ports	n	4
The dead zone of the main valve at the mid—position (mm)	Δ	0.62
The radius of the U-shaped valve orifice (mm)	R_v	1
The flow coefficient of the U-shaped valve orifice	C_{vd}	0.61
The velocity coefficient of the U-shaped valve orifice	C_{vv}	0.98
The jet angle of the U-shaped valve orifice (°)	θ_v	69

under various working conditions. Eventually, the parameters of the backstepping adaptive sliding mode control are determined as: $k_1 = 80\ 000$, $k_2 = 80\ 000$, $k_3 = 2000$, $k_4 = 100$, $c_1 = 100$, $c_2 = 100$, $d_1 = 0.000\ 05$. In addition, some key parameters of the simulation model are set as shown in table 1.

During the operation of the two-stage electro-hydraulic proportional valve, the parameters such as viscous damping coefficient, spring stiffness, spring preload and friction force will gradually change with the variations in the working environment. In this manuscript, it is assumed that these parameters follow a slowly varying pattern: the viscous damping coefficient B_v changes according to $B_v = B_{v0} + 0.1B_{v0}\sin(2\pi t)$, the spring stiffness k_v changes according to $k_v = k_{v0} + 0.1k_{v0}\sin(2\pi t)$, and the spring preload F_{vf} changes according to $F_{vf} = F_{vf0} + 0.1F_{vf0}\sin(2\pi t)$. In the simulation model, when tracking the displacement step signal with an amplitude of 4.5 mm, the tracking results of the main valve, the approaching process of the adaptive sliding mode surface and the adaptive estimation curve of the uncertain parameters are shown in figures 5 and 6, respectively.

The simulation results presented in figures 5 and 6 demonstrate that the designed adaptive backstepping sliding mode controller achieves asymptotic stability, while the adaptive estimation of uncertain parameters remains bounded despite system parameter uncertainty. The main valve exhibits rapid target displacement tracking, with a step response time of only 50 ms, and the steady-state tracking error is kept within 0.1 mm, confirming its excellent tracking performance.

To evaluate the effectiveness of the adaptive backstepping sliding mode control strategy proposed in this paper, a comparative analysis is performed between the backstepping sliding mode controller and the PWM controller. Similar to the parameter adjustment of the sliding mode adaptive controller, the MATLAB interface in Light software is utilized to rapidly construct the PID parameter adjustment model of the PWM controller. With the minimization of the tracking error of the valve core displacement under various working conditions as the objective, the genetic algorithm is adopted to automatically optimize and adjust the controller parameters. Eventually,

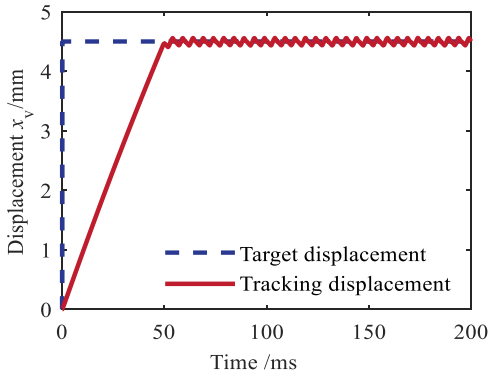

Figure 5. Simulation results of displacement tracking of power main spool under step signal.

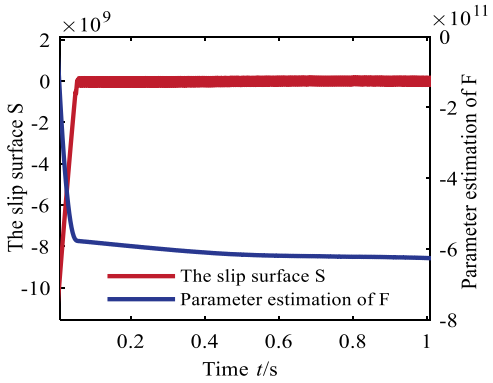

Figure 6. Sliding surface and uncertain parameter estimation curve.

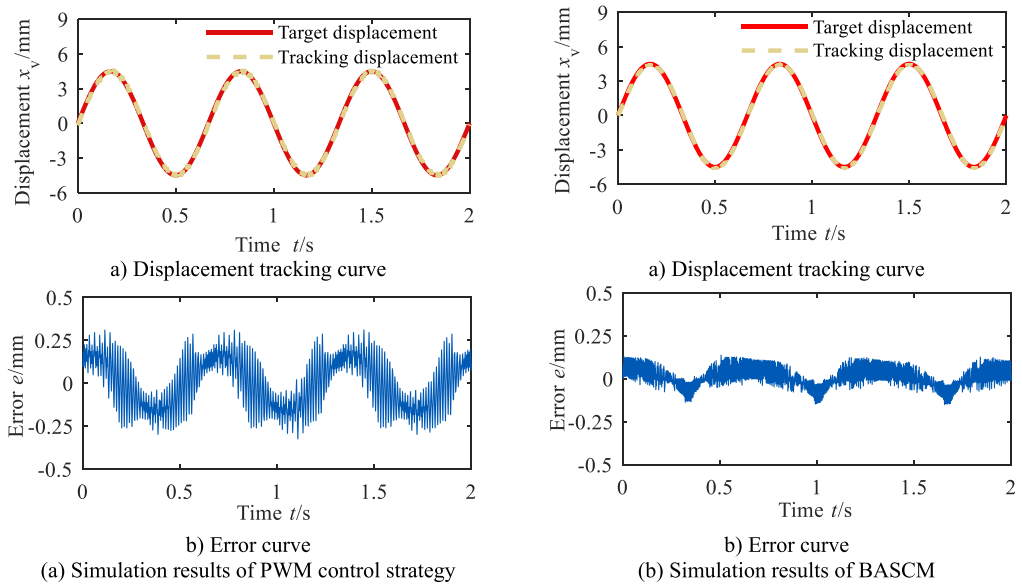

Figure 7. Simulation results of displacement control of DPPV under different control strategies.

the parameters of the PWM controller are determined as $K_p = 2300$ and $K_i = 3000$. In the simulation model, the desired displacement curve of the main valve spool follows a sinusoidal trajectory with an amplitude of 4.5 mm and a frequency of 1.5 Hz, expressed as $x = 4.5\sin(3\pi t)$. The simulation results comparing the two controllers are presented in figure 7.

Compared with the PWM controller, the main valve position tracking performance of the adaptive backstepping sliding mode controller shows a significant improvement.

Table 2. Comparative analysis of simulation results of two different types of controllers.

Controller	Maximum error M_e (mm)	Average error μ (mm)	Standard deviation σ(mm)
PWM	0.325	0.129	0.085
Adaptive Backstepping Sliding Mode	0.151(↓53.54%)	0.046(↓64.34%)	0.033(↓61.18%)

Specifically, the maximum error, average error and standard error are 0.151 mm, 0.046 mm and 0.033 mm, respectively, all of which are lower than those of the PWM controller. The reason for this improvement is that the backstepping adaptive sliding mode more controller fully accounts for the influence of external disturbances and unmodeled factors, thereby significantly enhancing the system's robustness and further optimizing the main valve's position tracking performance.

6. Experimental study

6.1. The principle and construction of test bench

To validate the effectiveness of the position servo control strategy for the main valve of a two-stage electro-hydraulic proportional valve, an experimental test system for the main valve position servo control is constructed using piezoelectric high-speed on/off valve pilot modulation, as depicted in figure 8. The experimental system primarily consists of a real-time control system (Lingshi Chuangqi Box-03), piezoelectric high-speed on/off valves, fixed orifices, a pilot stage oil circuit block, a three-position four-way slide valve (Hengli Hydraulic 4WRKE10E100L proportional directional valve main valve stage) with LVDT (model: SDC180–150, Test stroke: $\pm$7.5 mm, repeatability of displacement accuracy: 1%), a hydraulic power source, and a power amplifier (AETechron 7224), among other components.

The real-time control system is responsible for outputting the control signals to the piezoelectric high-speed on/off valve and collecting position signals in real time. The LVDT displacement sensor measures the position of the feedback main spool and transmits this data to the controller. The power amplifier amplifies the output signal from the real-time control system, enabling it to drive the piezoelectric high-speed on/off valve. Notably, the three piezoelectric stacks within the piezoelectric high-speed on/off valve are driven in parallel by the power amplifier. Additionally, the hydraulic power source operates at a pressure of 10 MPa and a flow rate of 8 l min^{-1}.

6.2. Analysis of experimental results

To thoroughly and scientifically evaluate and compare the effectiveness of different control strategies, this study designs three sets of experiments. Each set targets specific operating conditions, such as the sinusoidal position tracking of the main valve under variable amplitude and frequency conditions. The controller parameters used in the experiments are detailed in the previous section.

Condition 1: The main valve tracks a sinusoidal position signal with an amplitude of 4.5 mm and a frequency of 0.5 Hz, represented by $x = 4.5\sin(\pi t)$. The experimental comparison results for the three controllers are shown in figure 9.

As depicted in figure 9(a), when the PWM controller tracks a sinusoidal position signal with a frequency of 0.5 Hz, the maximum error, average error, and standard deviation of the main valve tracking are 0.323 mm, 0.116 mm, and 0.069 mm, respectively. The maximum error occurs near the peaks and troughs of the target position signal, where the valve spool displacement is largest, and the spring force is at its maximum, exerting a more significant impact on the main valve.

By comparing figures 9(a) and (b), it is clear that the backstepping adaptive sliding mode controller outperforms the PWM controller in terms of control performance. Specifically, the maximum error, average error, and standard deviation of the main valve tracking are reduced by 22.9%, 52.5%, and 43.5%, respectively. A detailed tracking comparison of the tracking metrics for the two controllers is shown in figure 12.

Condition 2: The main valve tracks a sinusoidal position signal, represented by $x = 4.5\sin(3\pi t)$. The experimental results for the three controllers are shown in figure 10.

As shown in figure 10(a), when the PWM controller tracks a sinusoidal position signal with a frequency of 1.5 Hz, the maximum error, average error, and standard deviation of the main valve tracking are 0.347 mm, 0.115 mm, and 0.077 mm, respectively. These values are similar to those observed when tracking the sinusoidal position with a frequency of 0.5 Hz.

As illustrated in figure 10(b), the backstepping adaptive sliding mode controller shows superior control performance compared to the PWM controller, similar to the results observed when tracking the 0.5 Hz sinusoidal position signal. Compared with the PWM controller, the most obvious advantage of the backstepping adaptive sliding mode controller is that it can reduce the maximum tracking error. The specific tracking comparison metrics for both controllers are shown in figure 12.

In addition, the tracking error of the spool displacement in the DPPV shows a small difference compared to the simulation results (as shown in table 2), which not only verifies the accuracy of the simulation model but also further proves the effectiveness of the sliding mode control method proposed in this paper.

Condition 3: The main valve tracks a sinusoidal position signal with an amplitude of 3 mm and a frequency of 1.5 Hz,

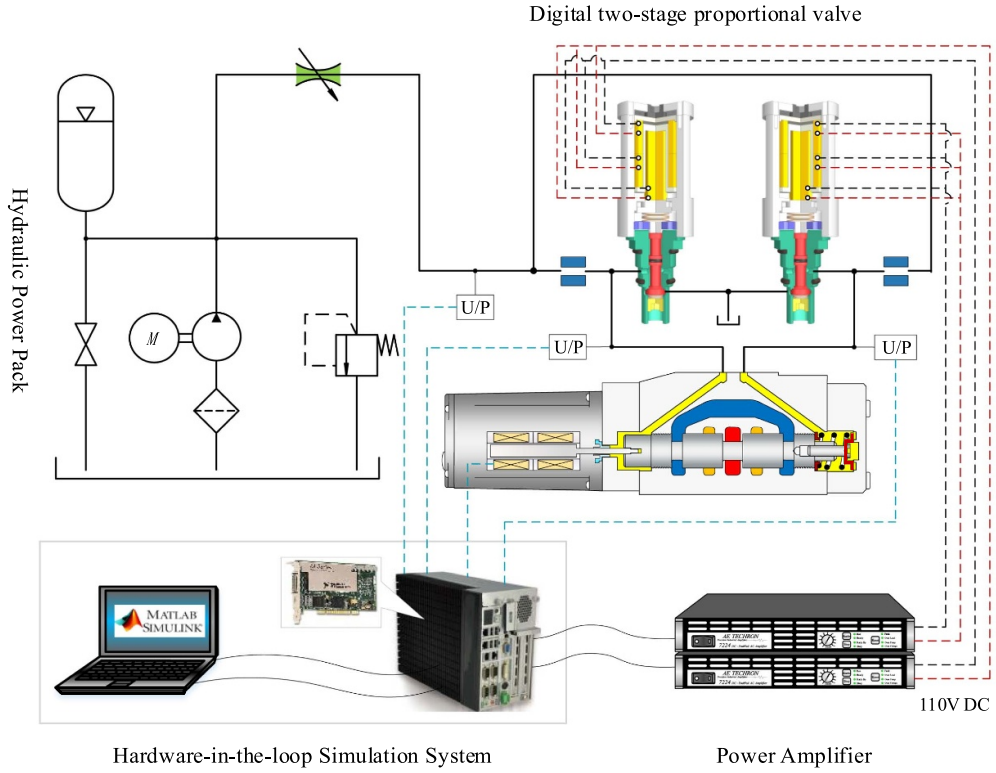

(a) Experimental schematic diagram

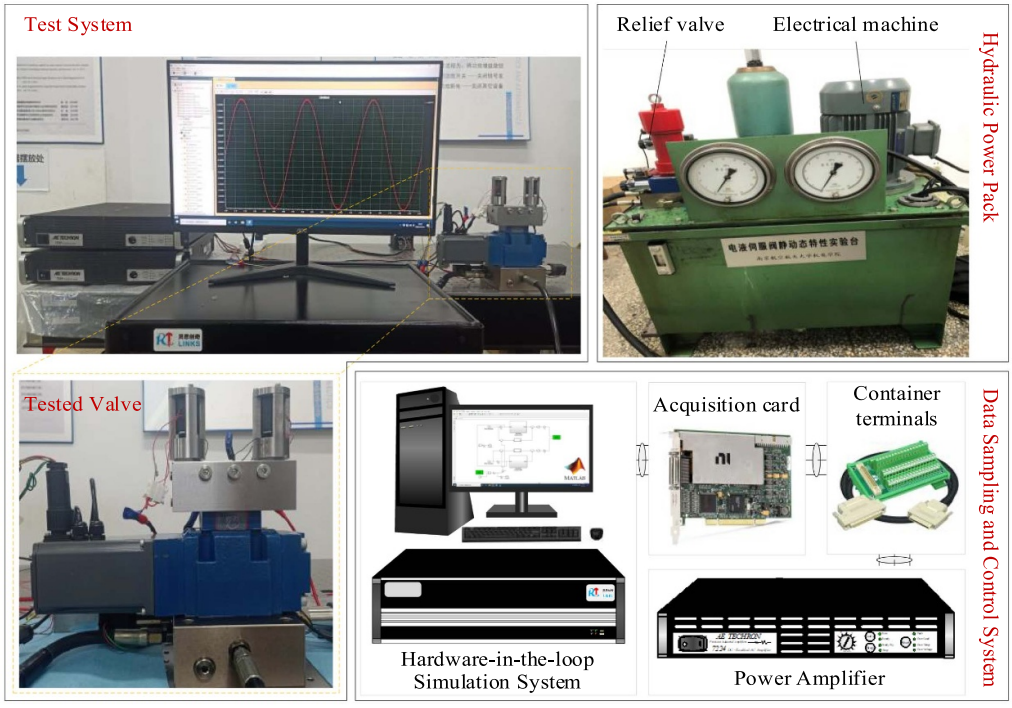

(b) Experimental system physical diagram

Figure 8. Experimental test system of main valve position servo control strategy.

represented by $x = 3\sin(3\pi t)$. The experimental results for the three controllers are presented in figure 11.

Compared with the second operating condition, the reduction in tracking amplitude leads to a smaller stroke of the main valve, weakening the effect of the spring force on the valve. As a result, the control performance of the backstepping adaptive sliding mode controller improves. For the PWM controller, the maximum error, average error, and standard deviation in main valve tracking are 0.337 mm, 0.122 mm, and 0.078 mm, respectively, indicating relatively poor control accuracy.

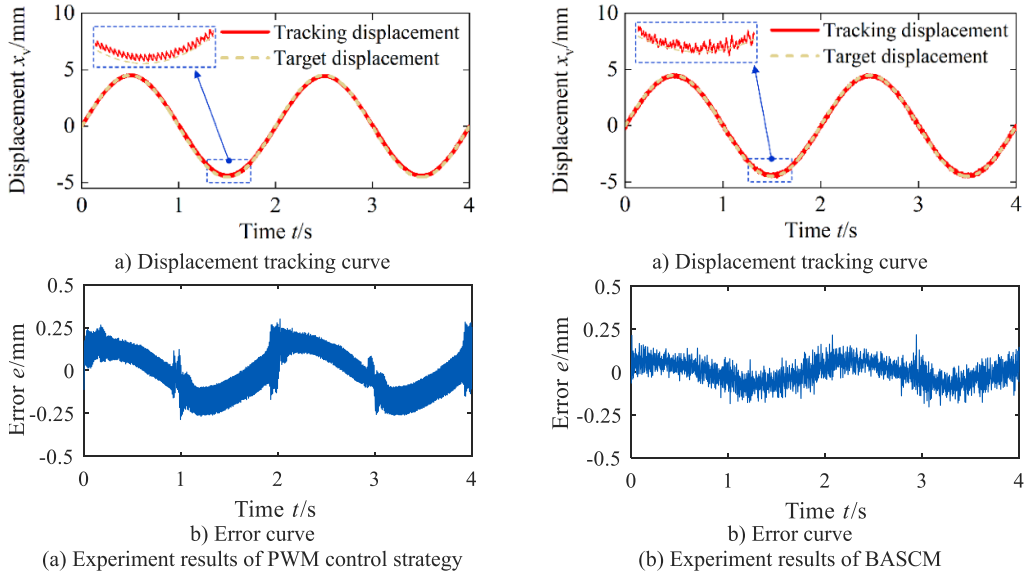

Figure 9. Experiment results of displacement control of DPPV under different control strategies (Condition 2: an amplitude of 4.5 mm and a frequency of 0.5 Hz, expressed as $x = 4.5\sin(\pi t)$).

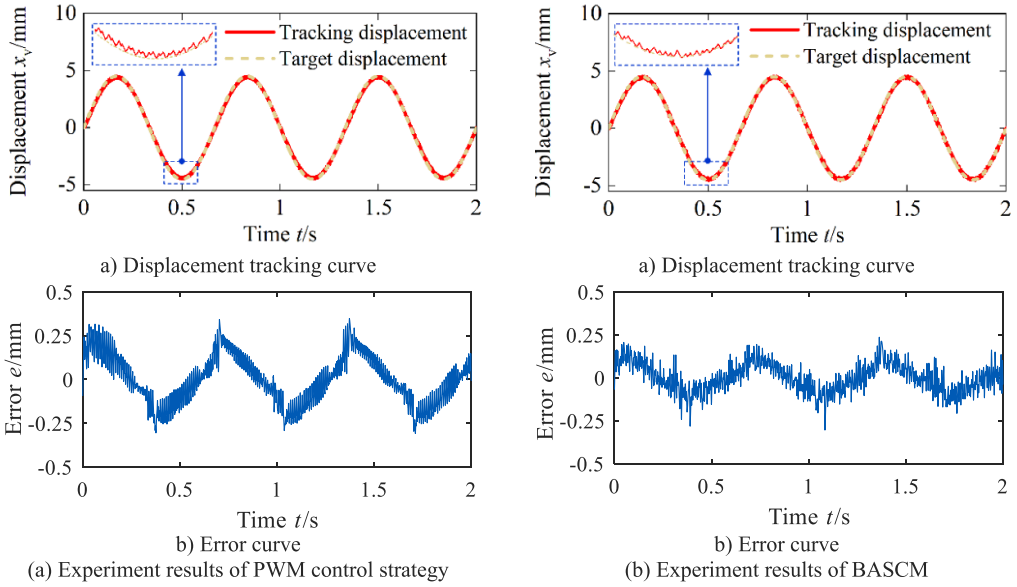

Figure 10. Experiment results of displacement control of DPPV under different control strategies (Condition 3: an amplitude of 4.5 mm and a frequency of 1.5 Hz, expressed as $x = 4.5\sin(3\pi t)$).

The specific tracking comparison indexes of the two controllers under different operating conditions are shown in figure 12. From the figure, it is clear that the PWM controller exhibits relatively poor control performance when tracking position signals with varying frequencies and amplitudes. The backstepping adaptive sliding mode controller, being a nonlinear control method, outperforms the PWM controller.

However, when comparing the experimental results with the simulation data, a performance gap is observed. This discrepancy is attributed to the high-frequency vibrations of the piezoelectric high speed on/off valve during the actual experiment. These vibrations cause changes in the relative position between the output rod and the valve core, leading to significant variations in dynamic response speed and static output flow, which ultimately resulting in performance that falls short of the simulation results.

Figure 13 presents a comparison of the valve spool displacement control accuracy between the DPPV proposed in this study and the digital two-stage valve with an array electromagnetic high-speed on/off valve,as the pilot drive, proposed by Dr Gao Qiang from Nanjing University of Aeronautics and Astronautics [38]. As clearly shown from the figure, under the tracking signal $x = 4.5\sin(3\pi t)$, the maximum error, average error, and standard deviation of the digital piezoelectric two-stage valve proposed in this study are significantly lower

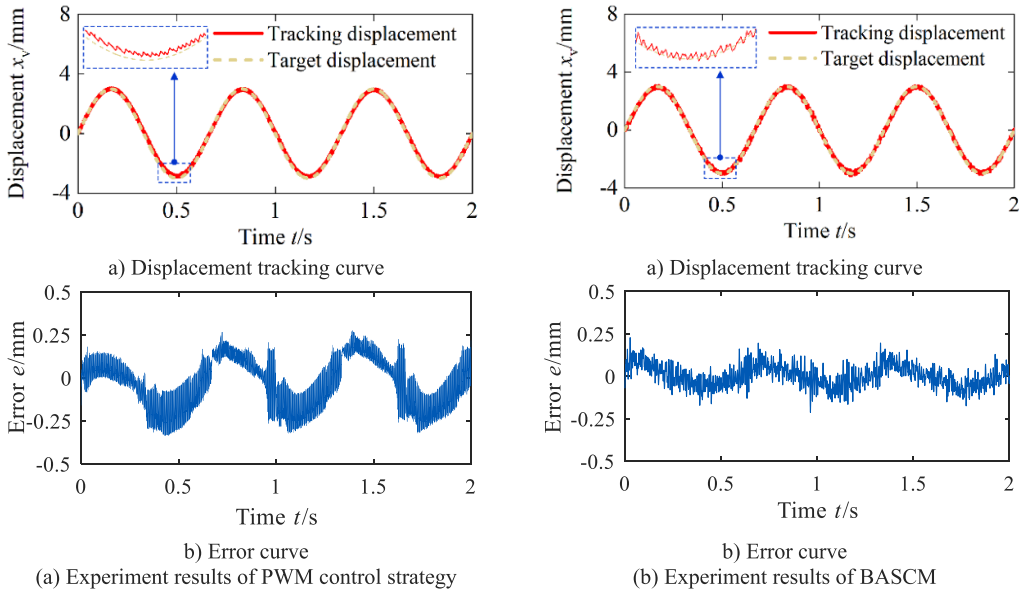

Figure 11. Experiment results of displacement control of DPPV under different control strategies (Condition 3: an amplitude of 3 mm and a frequency of 1.5 Hz, expressed as $x = 3\sin(3\pi t)$).

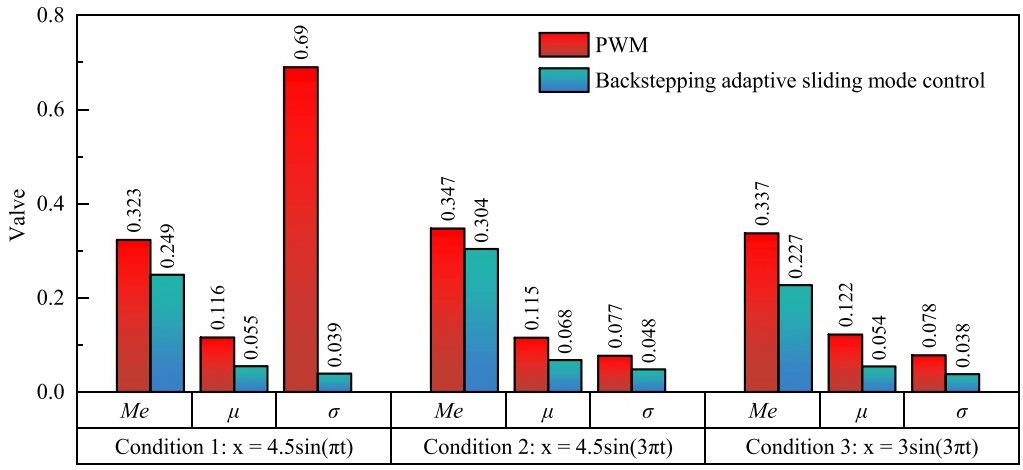

Figure 12. Experimental comparison of tracking error of different controllers (me: maximum (mm), μ: average error (mm), σ: standard deviation (mm)).

than those of the array electromagnetic high-speed on/off valve proposed by Dr Gao Qiang (which tracks the signal $x = 4.5\sin(4\pi t)$). This demonstrates the superior performance of the DPPV.

7. Discussion and conclusion

7.1. Discussion

Compared with the conventional PWM control strategy, the sliding mode adaptive control algorithm employed in this study effectively mitigates the effects of time-varying dynamics, unmodeled behavior, and unknown nonlinearities, significantly enhancing the control accuracy of the spool displacement. Nevertheless, both simulation and experimental results show noticeable fluctuations in the spool displacement, which adversely impact the stability and precision of subsequent pressure and flow control. To further improve the main spool's control performance, future research will explore the application of intelligent control methods, such as iterative learning control and robust control, for the displacement regulation of the DPPV, aiming to achieve higher accuracy and stronger robustness.

7.2. Conclusion

In this paper, a DPPV driven by a piezoelectric high-speed on/off valve with high dynamic and high flow resolution is designed. The structure and nonlinear dynamic model of the

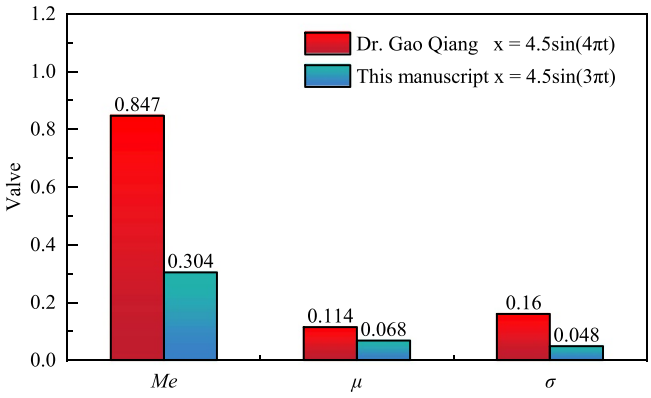

Figure 13. Comparison results of control accuracy of valve core displacement for different configurations of digital two-stage valves (me: maximum (mm), μ: average error (mm), σ: standard deviation (mm)).

DPPV are described. Furthermore, a backstepping adaptive sliding mode control strategy is developed to improve the control accuracy and anti-interference capability of the system.

The simulation and experimental results show that, when the backstepping adaptive sliding mode control strategy is employed instead of the traditional PWM control strategy, the maximum, average, and standard deviation of the tracking error are reduced by at least 12.3%, 40.8%, and 37.7%, respectively.

Compared to the digital proportional two-stage valve proposed by Dr Gao Qiang of Nanjing University of Aeronautics and Astronautics (NUAA), which uses an array of electromagnetic high-speed on/off valves as the pilot actuator (tracking curve: $x = 4.5\sin(4\pi t)$), the power main spool displacement tracking in this study (tracking curve: $x = 4.5\sin(3\pi t)$) demonstrates improvements of 64.1%, 40.35%, and 70% in maximum error, average error, and standard deviation, respectively.

Data availability statement

All data that support the findings of this study are included within the article (and any supplementary files).

Acknowledgments

The authors would like to thank the National Natural Science Foundation of China (No. 52375059) and Jiangsu Province Research and Practice Innovation Program (No. KYCX24_0554) for providing the funding for this research.

Author contributions

Linfei Li
Data curation (lead), Software (equal), Writing – original draft (equal)

Yuwen Wang
Data curation (supporting), Software (supporting)

Yuchuan Zhu 0000-0002-7399-1656
Funding acquisition (lead), Project administration (lead), Writing – review & editing (lead)

Jie Ling 0000-0002-6786-0422
Writing – review & editing (lead)

References

[1] Zhou Y, Hongju W, Jing Z and Hui B 2025 09544070241306248
[2] Hao Z, Wenshu W, Hong W, Yang Z and Xiaochao L 2025 *Actuators* **14** 11
[3] Qiwei Z, Xiangdong K, Bin Y, Kaixian B, Zhengguo J and Yan K 2020 *Appl. Sci.* **10** 579
[4] Sciatti F, Tamburrano P, Distaso E and Amirante R 2024 *Heliyon* **10** e27264
[5] Xin T, Xiaofan G, Patrick S, Giovanni D, Andrea V, Stefano F and Francesco P 2024 *Int. J. Fluid Power* **25** 203–24
[6] Nugraha G L, Ajis M, Adhi H S and Zakaria D 2024 *J. Mechatron. Artif. Intell.* **1** 27–44
[7] Linjama M 2011 Digital fluid power: State of the art *The 12th Scandinavian Int. Conf. on Fluid Power* vol 2 pp 18–20
[8] Qiang G, Shida Z and Yong Z 2023 *Aerospace* **10** 109
[9] Pei W, Yuxin Z, Matti L, Liying Z and Jing Y 2025 *Mech. Syst. Signal Process.* **224** 112201
[10] Scheidl R, Linjama M and Schmidt S 2012 *Proc. Inst. Mech. Eng. I* **226** 721–3
[11] Wei W, Zhiyuan L, Delai L, Yaoyao L and Wenbo Z 2024 *Mach. Tool Hydraul.* **52** 164–8
[12] Omberg C J and James P J 1994 USA
[13] Turner S B and Lakin D F 1996 UKP
[14] Eaton 2009 *Valvistor Cartridge Valve V-VLPO-MC011-E* (Eaton)
[15] Eaton 2016 *CMA200 technical document E-VLMB-BB002-E1* (Eaton)
[16] Danfoss 2017 *Proportional Valve Group 520L0344* (Danfoss Power Solutions Company)
[17] Yabin L 2023 *Msc* Lanzhou University of Technology (https://doi.org/10.27206/d.cnki.ggsgu.2023.000818)
[18] Gao Q, Lan B and Zhu Y 2024 *Proc. Inst. Mech. Eng. C* **238** 7015–28
[19] Qi Z 2019 *MSc Thesis* Zhejiang university
[20] Qi Z, Enguang X, Tiwei J, Huayong Y, Bin Z and Yanbiao L 2022 *J. Zhejiang Univ. Sci. A* **23** 272–85
[21] Long X 2020 *MSc Thesis* Lanzhou university of technology
[22] Long X, Liejiang W, Zhuang N, Li W and Yinshui L 2019 *Proc. 2019 Int. Conf. on Fluid Power and Mechatronics—FPM*
[23] Qiang G, Yuchuan Z, Changwen W and Yulei J 2021 *Front. Mech. Eng.* **16** 420–34
[24] Heng Z, Yaoyao L, Ze T, Zisheng L and Ruihao Z 2022 *Machines* **10** 37
[25] Ruihao Z, Yaoyao L, Zisheng L, Runze L and Yongchang G 2021 *Proc. Inst. Mech. Eng. E* **235** 1930–44
[26] Ruihao Z, Yaoyao L and Zisheng L 2021 *The 10th Int. Conf. on Fluid Power Transmission and Control* pp 507–11
[27] Fan D, Jiandi Y, Jing D, Jian C and Ce Z 2011 *Chin. J. Constr. Mach.* **9** 351–8
[28] Qi Z, Xianjian H, Yanbiao L, Bin Z, Huayong Y and Bo C 2021 *J. Mech. Eng.* **57** 224–35
[29] Yuzhou D, Jie L, Micky R and Yuchuan Z 2025 *Smart Mater. Struct.* **34** 045022
[30] Rui W, Yuchuan Z, Yulei J and Long C 2020 *Smart Mater. Struct.* **29** 035003

[31] Qin L, Zhiei R, Liang G and Chenyang D 2024 *Mech. Syst. Signal Process.* **208** 110964
[32] Jie L, Long C, Mingming Z and Yuchuan Z 2023 *Smart Mater. Struct.* **32** 025011
[33] Zhang J, Lu Z, Xu B and Su Q 2019 *ISA Trans.* **93** 218–30
[34] Li Q, Ruan Z and Ding C 2025 *Control Eng. Pract.* **162** 106365
[35] Zhao F, Min M, Jie L, Xiaohui X, Zhixin Y and Feng W 2022 *Mech. Syst. Signal Process.* **164** 108249
[36] Wang Z and Guan G 2025 *J. Vib. Control* **31** 1524–35
[37] Baoquan J, Shibo X and Hang C 2013 *J. Mech. Eng.* **49** 163–9
[38] Gao Q, Liu H, Lan B and Zhu Y 2024 *ISA Trans.* **151** 312–23